4-2014

Magnetic properties of Fe-doped MnAl

Priyanka Manchanda
University of Nebraska-Lincoln, pmanchanda2@unl.edu

Arti Kashyap
The LMN Institute of Information Technology, akashyap@lnmiit.ac.in

Jeffrey E. Shield
University of Nebraska-Lincoln, jshield2@unl.edu

L. H. Lewis
Northeastern University, lhlewis@neu.edu

Ralph Skomski
University of Nebraska-Lincoln, rskomski2@unl.edu

Published in *Journal of Magnetism and Magnetic Materials* 365 (2014), pp. 88–92
doi: 10.1016/j.jmmm.2014.04.007

Submitted January 17, 2014; revised March 21, 2014; published online April 15, 2014.

Magnetic properties of Fe-doped MnAl

P. Manchanda,[1, 2] A. Kashyap,[2] J. E. Shield,[3] L. H. Lewis,[4] and R. Skomski[1]

1. Department of Physics and Astronomy and Nebraska Center for Materials and Nanoscience, University of Nebraska, Lincoln, NE 68588, USA
2. School of Basic Sciences, Indian Institute of Technology Mandi, HP, India 175001
3. Department of Mechanical and Materials Engineering, University of Nebraska— Lincoln, NE 68503, USA
4. Department of Chemical Engineering, Northeastern University, Boston, MA 02115, USA

Corresponding author – R. Skomski, email rskomski@unl.edu

Abstract

Electronic and magnetic properties of $L1_0$-ordered $Fe_xMn_{1-x}Al$ alloys (x=0, 0.0625, 0.125, 0.1875, 0.5) are investigated by first-principle supercell calculations. Pristine MnAl exhibits robust ferromagnetism involving the dense-packed Mn atoms in (001) planes of the tetragonal structure. Iron substitution for Mn significantly deteriorates the magnetization of the alloy. The reduction is a dilution effect, caused by the relatively small Fe moment of about 1.9 μ_B per atom, as compared to the Mn moment, which exceeds 2.4 μ_B. By contrast, 50% Fe substituted for Mn (x=0.5) yields a magnetocrystalline anisotropy enhancement of about 40%. Both the magnetization reduction and the anisotropy enhancement mainly arise due to the change in d_{xy} and d_{zx} minority density of states (DOS) at the Fermi level.

1. Introduction

Manganese (Mn^{+2}) has a maximum magnetic moment of 5 μ_B per atom. If the local (atomic) moment of Mn could be exploited in industrial magnets, it could revolutionize permanent magnet technology and open the door for completely new technologies. Furthermore, Mn is a relatively inexpensive metal, which is of utmost importance in light of the current tight supply and high cost of the rare-earth elements that are used in current advanced magnets [1]. Unfortunately, most manganese compounds are antiferromagnetic, which is typical for compounds formed from elements in the middle of the 3*d* series [2, 3]. This situation precludes the use of Mn in many applications that require ferromagnetic materials. For example, MnPt alloys with the tetragonal $L1_0$ structure are antiferromagnetic with high Néel temperatures resulting from antiparallel coupling between adjacent Mn atom located in (001)-planes [4]. Similarly, MnRh, MnPd, MnIr and MnNi alloys are also antiferromagnetic [2]. It is important to understand how the magnetic properties of Mn-based compounds depend upon chemical and structural details.

Chemically-ordered, equiatomic $L1_0$-structured MnAl, also known as τ-phase MnAl, is one of the few ferromagnetic manganese-containing compounds and has been studied since late 1950s [5] and [6]. The MnAl τ-phase alloy is a good candidate for permanent magnet applications, because it exhibits appreciable intrinsic properties, $\mu_o M_s$=0.75 T, K_1=1.7 MJ/$m^3$and T_c=650 K [7] and [8], with a theoretical maximum energy product at room temperature of 112 KJ/m^3 (14 MGOe) [1]. The intrinsic magnetic properties of MnAl are superior or comparable to those of hard ferrites such as barium hexaferrite and of alnicos but not as good as those of rare-earth magnets or of FePt and CoPt equiatomic ordered alloys [1, 7, 8]. However, one disadvantage of τ-phase MnAl is its structural instability at room temperature [9]. τ-phase MnAl is formed from the metastable hexagonal high-temperature ε-MnAl parent phase by annealing at about 500 °C. The ε-phase of MnAl is antiferromagnetic with a Néel temperature T_N of 90 K [10]. The metastable $L1_0$ phase decomposes into a solid solution of γ(Al_8Mn_5) and β-(Mn) phases, but small additions of carbon are confirmed to drastically improve the stability of the $L1_0$ phase [11]. Despite these complications, both Mn and Al are cheap and readily available, and there are many potential applications that are well suited for MnAl magnets.

The importance of chemical additives in MnAl has been known for a long time. For example, the stability and magnetic properties of MnAl alloys with doping of C, B and rare earth elements have been investigated. Carbon stabilizes the MnAl $L1_0$ structure but reduces the Curie temperature while B does not stabilize the MnAl structure at all [12]. Zeng et al. reported that additions of C into $L1_0$-type MnAl increase the saturation magnetization and reduce the anisotropy field [10]. It has been found that the substitution of Zn stabilizes the $L1_0$ structure in MnAl and increases the coercivity and magnetization but reduces the Curie temperature [13]. The substitution of Ni in MnAl has also been investigated and it has been found that both magnetization and coercivity increases with Ni content [14]. The effect of Fe addition on the magnetic properties of τ-phase MnAl has been investigated experimentally [15]. These investigations indicate that the Curie tem-

perature increases with increasing Fe concentration, confirming that Fe doping strongly affects the structural and magnetic properties of MnAl alloys. In this work, we use first-principle calculations to study the effect of Fe substitution on the magnetic properties of MnAl alloys. Our results demonstrate that Fe substitution for Mn in τ-phase MnAl enhances the magnetic anisotropy energy but decreases the saturation magnetization.

2. Computational details

The calculations are performed using a frozen-core full-potential projected augumented wave (PAW) method [16], as implemented in the Vienna *ab-initio* simulation package (VASP) [17]. The electronic exchange and correlation effect are described within the generalized-gradient approximation (GGA), using the functional proposed by Perdew et al. [18]. The energy cutoff of the plane wave basis set is taken as 450 eV. For all the calculations, the experimental lattice parameter of MnAl is used (a=3.93 Å, c=3.56 Å) and energy convergence is set at 10^{-6}. The optimized value of cut-off energy is taken to be 450 eV. Figure 1 shows the supercell used in the calculations, which consists of 32 atoms.

In our calculations, we assume that Fe substitutes for Mn, as suggested by the reported atomic radii of 1.43 Å for Al, 1.26 Å for Mn, and 1.27 Å for Fe [19]. The electronic structure, magnetic moment and magnetic anisotropy of $Fe_xMn_{1-x}Al$ alloys (x=0.0625, 0.1250, 0.1875, 0.500) are calculated. To compute the magnetic anisotropy energy, 512 k-points are used in the irreducible part of Brillouin zone. The convergence of energy with respect to the number of k-points has been carefully checked, with the finding that 512 k-points are sufficient to calculate the magnetic anisotropy energy accurately.

3. Results and discussion

Table 1 shows the calculated average moments of Fe, Mn and Al as well as the total magnetic moments for all investigated MnAl stoichiometries. In pure $L1_0$-ordered MnAl, the calculated moments of Mn and Al atoms are 2.44 μ_B and

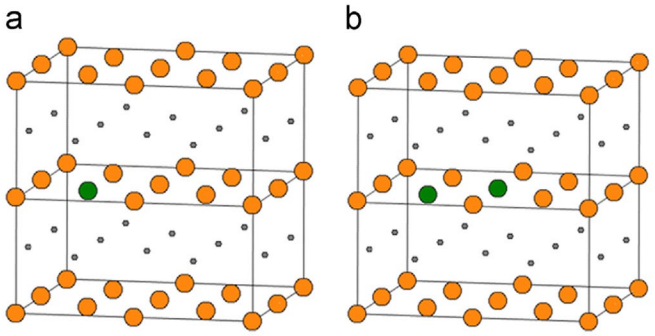

Figure 1. Typical $Fe_xMn_{1-x}Al$ supercell structures: (a) x=0.0625 and (b) x=0.125.

Table 1. Total magnetic moments, average atomic magnetic moments and magnetic anisotropy energies of the investigated Fe–Mn–Al.

	Total (μ_B)	⟨Fe⟩ (μ_B)	⟨Mn⟩ (μ_B)	⟨Al⟩ (μ_B)	K_1 (meV/supercell)
$Mn_{16}Al_{16}$	38.06	–	2.44	−0.061	4.855
$Mn_{15}FeAl_{16}$	37.608	1.886	2.445	−0.06	5.047
$Mn_{14}Fe_2Al_{16}$	37.023	1.885	2.443	−0.059	5.189
$Mn_{13}Fe_3Al_{16}$	36.754	1.924	2.455	−0.058	5.416
$Mn_8Fe_8Al_{16}$	34.008	1.899	2.461	−0.056	6.968

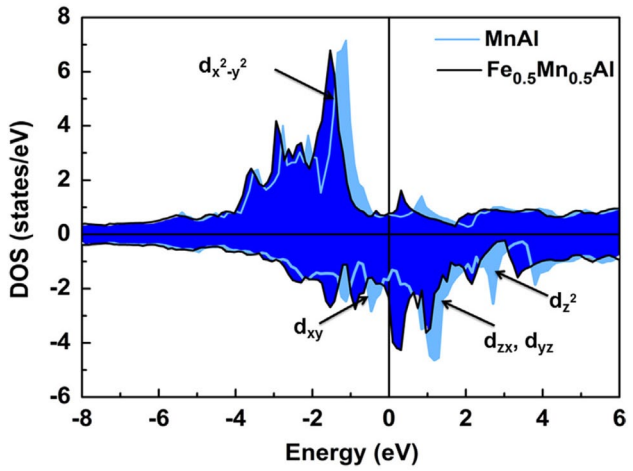

Figure 2. Calculated total DOS for MnAl and $Fe_{0.5}Mn_{0.5}Al$. Positive and negative values on the vertical axis indicates the density in majority and minority spin states, respectively. The arrows indicate the predominant character of the peaks.

−0.061 μ_B, respectively, indicating antiferromagnetic coupling between Mn and Al sublattices. The experimental saturation magnetization of Fe-free MnAl, 0.7 T is lower than the calculated magnetization (1.0 T), very likely due to Mn antisite disorder. In Table 1, the off-stoichiometric compositions $Mn_{15}FeAl_{16}$, $Mn_{14}Fe_2Al_{16}$, $Mn_{13}Fe_3Al_{16}$ and $FeMnAl_2$ correspond to Fe concentrations of 6.25%, 12.5%, 18.75% and 50%, respectively.

Table 1 shows that the total magnetic moment of the supercell becomes smaller as the Fe concentration increases. However, in contrast to the situation manifest in Fe-substituted MnBi thin films [22], the experimentally-confirmed Curie temperature enhancement supports the absence of antiferromagnetic interatomic exchange between Fe and Mn. In fact, we have found a local magnetic moment value of 1.9 μ_B for Fe (somewhat reduced from the bulk value of 2.2 μ_B per Fe atom) and Mn is 2.45 μ_B. This indicates that the moment reduction is a "dilution" effect, caused by the substitution of Fe for Mn.

Further insight into the origin of Fe and Mn magnetic moment is provided by the computed densities of states (DOS). Figure 2 shows the total densities of states of MnAl and $Fe_{0.5}Mn_{0.5}Al$. Compared to MnAl, the states of $Fe_{0.5}Mn_{0.5}Al$ are shifted to lower energies which is a band-filling effect. Since Fe has one electron more than Mn which enhances the minority DOS in the vicinity of the Fermi level. This results in the reduction of magnetic moment in $Fe_{0.5}Mn_{0.5}Al$ compared to MnAl.

Figure 3 shows the element-specific partial densities of states (PDOS) in $Fe_{0.5}Mn_{0.5}Al$. We find almost completely filled majority d bands for both Fe and Mn atoms whereas the minority bands are partially occupied (strong ferromagnetism). The d bands of Fe and Mn strongly hybridize, and the exchange splitting of Fe DOS is smaller than that of Mn, resulting in a smaller magnetic moment per Fe atom and a reduced total magnetic moment. For all compositions, there is also some negative contribution to the magnetic moment due to the p-electrons of Al atom. At the Fermi level, the minority DOS (↓) is much larger than the majority DOS (↑). This means that additional Fe substitution for Mn would yield extra d electrons that go predominantly into the minority band and further reduce the overall magnetization. This approximately linear dependence of the total moment on the Fe concentration is also evident from Table 1.

The magnetic anisotropy energies of MnAl and $Fe_xMn_{1-x}Al$ are calculated by comparing the energy differences between in-plane and perpendicular magnetization directions. The

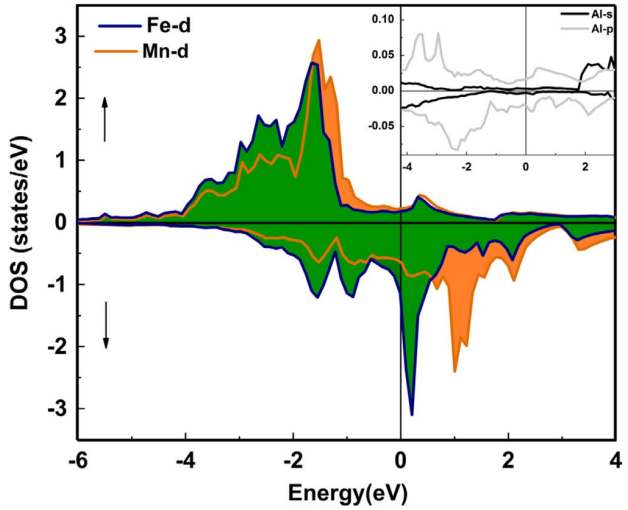

Figure 3. Spin-polarized majority (↑) and minority (↓) *d*-band densities of states (DOS) of $MnFeAl_2$ relative to the Fermi level. The inset shows the *s*- and *p*-band DOS of Al.

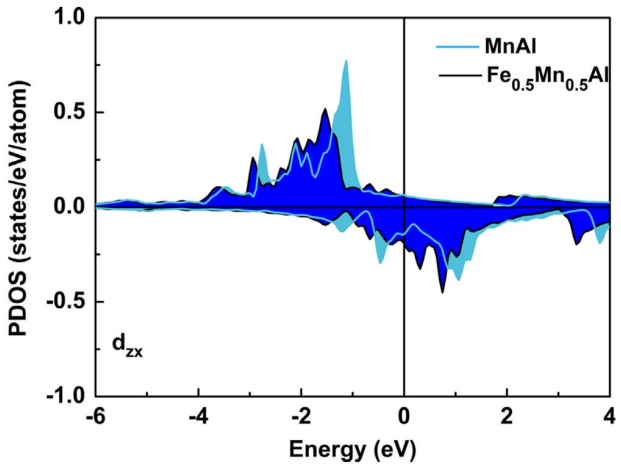

Figure 4. Partial DOS for the d_{zx} bands in MnAl and $Fe_{0.5}Mn_{0.5}Al$.

calculated magnetic anisotropy for bulk $L1_0$-MnAl is 0.62 meV/unit cell, or K_1=1.77 MJ/m^3. This is in agreement with previous theoretical and experimental results [7, 20, 21]. Notably the calculated magnetic anisotropy energy is 1.5 MJ/m^3 using an LMTO method [20].

Iron substitution in MnAl enhances the anisotropy up to 2.5 MJ/m^3 for $Mn_8Fe_8Al_{16}$, as shown in the last row of Table 1. This is because an Fe atom has one extra 3*d* electron compared to Mn and the magnetic anisotropy strongly depends on the number of electrons in the system. In Ref. [23] and [24] it has been argued that the magnetic anisotropy increases with the number of valence electrons, reaching a maximum for 8 valence electrons and decreasing towards the end of the series. In Mn and Fe the valence electron configuration is $3d^5 4s^2$ and $3d^6 4s^2$ with the total number of valence electrons 7 and 8, respectively. However, such rules are very crude, and the magnetocrystalline anisotropy generally oscillates as an atomic-structure-dependent function of the *d*-band filling [25–27].

An alternative way of rationalizing the trend found for magnetic anisotropy in MnAl is second-order perturbation theory [28]. In this approximation, the anisotropy is caused by matrix elements or coupling of the spin–orbit interaction between occupied and unoccupied states and is inversely proportional to the energy difference between occupied and unoccupied *k* states, $K_1 \sim 1/(E_o - E_u)$. The partial DOS of Figure 3 shows that the majority states are almost fully occupied, so that the anisotropy is mainly determined by coupling between the minority states, with a smaller contribution attributed to matrix elements between majority and minority states. The shapes of Mn DOS in MnAl and in $Fe_{0.5}Mn_{0.5}Al$ are very similar, but there is a small difference in the position of peaks.

Near the Fermi level, where the $E_o - E_u$ is smallest, the DOS is larger for $Fe_{0.5}Mn_{0.5}Al$ than for MnAl, corresponding to an enhanced number of states that contribute to the anisotropy in the Fe-modified compound. There are virtually no $d_{x^2-y^2}$ states at the Fermi level for either compound, but the other subbands, especially d_{yx} and d_{zx}, lies at the Fermi level and therefore contributes to anisotropy. Figure 4 illustrates this situation by showing the partial DOS for the d_{zx} band in both compounds.

It is instructive to discuss how atomic-scale disorder is described by various theoretical approaches. Let us consider an equiatomic *AB* alloy where *A* atoms (yellow) and *B* atoms (red) have on-site atomic energies of $\pm E_o$, respectively, Figure 5(a). The simplest approach to disorder is the virtual-crystal approximation (VCA), where the on-site potential is averaged over all *A* and *B* atoms, as illustrated in Figure 5(b). This approach is trivial from the viewpoint of density of states, which is assimilated to that of a monatomic metal, as in the closely related rigid-band model [29]. The shortcomings of this approximation can be seen very easily by considering the limit of large on-site energy splittings E_o, where the "red" *B* atoms have much lower energies than the "yellow" *A* atoms. In this limit, the interatomic hopping integral $|t|$ is much smaller than E_o, and the DOS effectively splits into two bands or narrowly-spaced level groups centered around $\pm E_o$, in striking contrast to a single band corresponding to Figure 5(b).

A major improvement is provided by the coherent-potential approximation (CPA), where the alloy behavior is deduced by properly distinguishing between *A* and *B* atoms on any given site but treating the neighboring atoms as an effective medium [29–31]. In terms of Figure 5, the CPA amounts to a weighted average between *A* atoms (c) and *B* atoms (c), very similar to the mean-field approximation in statistical physics but requiring a more complicated treatment of the individual electron states.

The present supercell approach is an advanced but potentially time-consuming method. A small chunk of material—for example the bright 3×3 region in Figure 5(a)—is repeated periodically. This makes it possible to exploit the Bloch theorem and the accuracy of the calculation (including the resolution of the chemical concentration) is limited by the supercell size only. Compared to the CPA, supercell calculations have the advantage of correctly describing cluster-localization effects [30, 32]. An example of such a cluster is the dark region of six low-energy *B* or "red" atoms in the top-left corner of Figure 5(a). If the *AB* alloy is filled with electrons, then the first electrons go into "red" or *B* clusters, where they benefit from both the low on-site energy and from the freedom to hop around in *B*-metal mini regions. This hopping effect is poorly described in single-site approximations such as the CPA [30, 32].

In the present paper, the biggest supercell contain 16 formula units of MnAl. This makes it possible to resolve defect concentrations with a resolution of about 3%. For one Fe atom per supercell, there is only one non-equivalent configuration Figure 1(a). For two Fe atoms per unit cell, there are 7 non-equivalent configurations, as previously analyzed for isostructural Fe–Co–Pt [33]. Figure 1(b) shows one of these configurations, where the defected atoms are nearest neighbors and exhibit a hopping contribution that is not accurately described

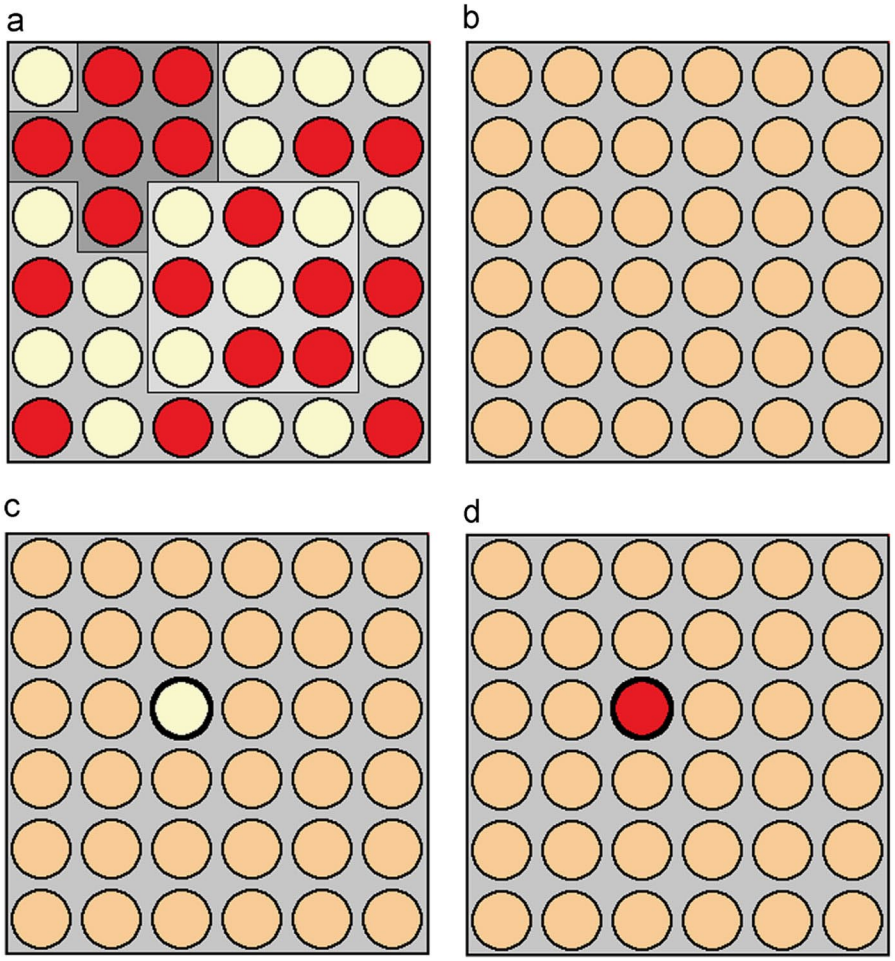

Figure 5. Theoretical approaches to metallic disorder: (a) *AB* alloy with atoms having onsite energies of $+E_o$ (bright yellow, *A*) and $-E_o$ (dark red, *B*), (b) virtual-crystal approximation and (c and d) coherent potential approximation. In (a), the bright 3×3 square in the center symbolizes a supercell calculation, whereas the dark region (top left) symbolizes a cluster ignored in the CPA.

by the CPA. For higher concentrations, the ensemble averaging becomes time-consuming, but it is then possible to exploit the self-averaging of the electronic structure [29] of the considered alloys.

4. Conclusions

In summary, we have studied the magnetic properties of MnAl alloys and the effect of Fe substitution on the magnetic properties of MnAl alloys. We find MnAl to exhibit robust ferromagnetism, in spite of the very short Mn–Mn distances, but Fe addition reduces the net magnetization, because the average moment per transition-metal atom is decreased. By contrast, Fe improves the magnetocrystalline anisotropy, a feature linked to the enhancement of the minority density of states at the Fermi level. This makes Fe substitutions in MnAl alloys an interesting tool to tailor intrinsic magnetic properties and to enhance the magnetic anisotropy and coercivity of the material.

References

[1] J.M.D. Coey Permanent magnets: plugging the gap Scr. Mater., 67 (2012), pp. 524–529

[2] R.Y. Umetsu, A. Sakuma, K. Fukamichi Magnetic anisotropy energy of antiferromagnetic $L1_0$-type equiatomic Mn alloys Appl. Phys. Lett., 89 (2006), pp. 052504-1–052504-3

[3] A. Sakuma, R.Y. Umetsu, K. Fukamichi Magnetic structures and their stability in Mn_3Rh ordered and disordered alloys Phys. Rev. B, 66 (2002), pp. 014432-1–014432-6

[4] Z. Lu, R.V. Chepulskii, W.H. Butler First-principle study of magnetic properties of $L1_0$-ordered MnPt and FePt alloys Phys. Rev. B, 81 (2010), pp. 094437-1–094437-8

[5] H. Kono On the ferromagnetic phase in manganese–aluminum system J. Phys. Soc. Jpn., 13 (1958), pp. 1444–1451

[6] A.J.J. Koch, P. Hokkeling, M.G.V.D. Sterg, K.J. DeVos New material for permanent magnets on a base of Mn and Al J. Appl. Phys., 31 (1960) (71S-1–71S-3)

[7] J.M.D. Coey Hard magnetic materials: a perspective IEEE Trans. Magn., 47 (2011), pp. 4671–4681

[8] R. Skomski, J.M.D. Coey Permanent MagnetismInstitute of Physics, Bristol (1999)

[9] Y. Kurtulus,and, R. Dronskowski Electronic structure, chemical bonding, and spin polarization in ferromagnetic MnAl J. Solid State Chem., 176 (2003), pp. 390–399

[10] K. Kamino, T. Kawaguchi, M. Nagakura Magnetic properties of MnAl system alloys IEEE Trans. Magn., 2 (1966), pp. 506–510

[11] Q. Zeng, I. Baker, J.B. Cui, Z.C. Yan Structural and magnetic properties of nanostructured Mn–Al–C magnetic materials J. Magn. Magn. Mater., 308 (2007), pp. 214–226

[12] Z.W. Liu, C. Chen, Z.G. Zheng, B.H. Tan, R.V. Ramanujan Phase transitions and hard magnetic properties for rapidly solidified MnAl alloys doped with C, B, and rare earth elements J. Mater. Sci., 47 (2012), pp. 2333–2338

[13] H.X. Wang, P.Z. Si, W. Jiang, J.G. Lee, C.J. Choi, J.J. Liu, Q. Wu, M. Zhong, H.L. Ge Structural stabilizing effect of Zn substitution on MnAl and its magnetic properties Open J. Microphys., 1 (2011), pp. 19–22

[14] M. Matsumoto, A. Morisako, N. Kohshiro Crystal structure and magnetic properties of Mn–Al–Ni ferromagnetic films IEEE Transl. J. Magn. Jpn., 6 (1991), pp. 134–140

[15] C. Paduani, J. Schaf, A.I.C. Persiano, J.D. Ardisson Investigation of ferromagnetism in $Mn_{1-x}Al_{1-y}Fe_{x+y}$ alloys J. Alloys Compd., 479 (2005), pp. 1–5 View Record in Scopus

[16] G. Kresse, D. Joubert From ultrasoft pseudopotentials to the projector augumented-wave method Phys. Rev. B, 59 (1999), pp. 1758–1775

[17] G. Kresse, J. Hafner *Ab initio* molecular dynamics for open-shell transition metals Phys. Rev. B, 48 (1993), pp. 13115–13118

[18] Y. Wang, J.P. Perdew Correlation hole of the spin-polarized electron gas, with exact small-wave-vector and high-density scaling Phys. Rev. B, 44 (1991), p. 13298

[19] C. Kittel Introduction to solid state physics, Wiley, New York (1968)

[20] A. Sakuma Electronic structure and magnetocrystalline anisotropy energy of MnAl J. Phys. Soc. Jpn., 63 (1994), pp. 1422–1428

[21] J.H. Park, Y.K. Hong, S. Bae, J.J. Lee, J. Jalli, G.S. Abo, N. Neveu, S.G. Kim, C.J. Choi, J.G. Lee Saturation magnetization and crystalline anisotropy calculations for MnAl permanent magnet J. Appl. Phys., 107 (2010) (09A731-1–09A731-3)

[22] P. Kharel, X.Z. Li, V.R. Shah, N. Al-Aqtash, K. Tarawneh, R.F. Sabirianov, R. Skomaki, D.J. Sellmyer Structural, magnetic, and electron transport properties of MnBi:Fe thin films J. Appl. Phys., 111 (2012) (07E326-1–07E326-3)

[23] G. Meyer, J.-U. Thiele Effective electron-density dependence of the magnetocrystalline anisotropy in highly chemically ordered pseudobinary $(Fe_{1-x}Mn_x)_{50}Pt_{50}$ $L1_0$ alloys Phys. Rev. B, 73 (2006), pp. 214438-1–214438-7

[24] T. Suzuki, H. Kanazawa, A. Sakuma Magnetic and structural properties of quaternary $(Fe–Co–Ni)_{50}Pt_{50}$ alloy thin films IEEE Trans. Magn., 38 (2002), pp. 2794–2795

[25] D.-Sh Wang, R.-Q. Wu, A.J. Freeman First-principle theory of surface magnetocrystalline anisotropy and the diatomic-pair model Phys. Rev. B, 47 (1993), pp. 14932–14947

[26] R. Skomski, A. Kashyap, A. Solanki, A. Enders, D.J. Sellmyer Magnetic anisotropy in itinerant magnets J. Appl. Phys., 107 (2010) (09A735-1–09A735-3)

[27] R. Skomski, P. Manchanda, P. Kumar, B. Balamurugan, A. Kashyap, D.J. Sellmyer Predicting the future of permanent-magnet materials IEEE Trans. Magn., 49 (7) (2013), pp. 3215–3220

[28] P. Bruno Tight-binding approach to the orbital magnetic moment and magnetocrystalline anisotropy of transition-metal monolayers Phys. Rev. B, 39 (1989), pp. 865–868

[29] A. Gonis Theoretical Materials Science Materials Research Society, Warrendale, PA (2000)

[30] E.N. Economou Green's functions in quantum physics, Springer, Berlin (1979)

[31] P. Soven Coherent-potential model of substitutional disordered alloys Phys. Rev., 156 (1967), pp. 809–813

[32] R. Skomski Phase formation in $L1_0$ magnets J. Appl. Phys., 101 (2007) (09N517-1–09N517-3)

[33] P. Manchanda, P. Kumar, A. Kashyap, M.J. Lucis, J.E. Shield, A. Mubarok, J. Goldstein, S. Constantinides, K. Barmak, L.-H. Lewis, D.J. Sellmyer, R. Skomski Intrinsic properties of Fe-substituted $L1_0$ magnets IEEE Trans. Magn., 49 (10) (2013), pp. 5194–5198